A COMPARISON OF TIME-OPTIMAL INTERCEPT TRAJECTORIES FOR THE F-8 AND F-15 - FINAL REPORT

January, 1990

Research Supported by
NASA Ames/Dryden Flight Research Facility
Grant No. NCC 2-506

Principal Investigator: Dr. Anthony J. Calise
Research Assistant: James B. Pettengill
NASA Grant Monitor: Eugene L. Duke

Georgia Institute of Technology
School of Aerospace Engineering
Atlanta, GA 30332

A COMPARISON OF TIME-OPTIMAL INTERCEPT TRAJECTORIES FOR THE F-8 AND F-15 - FINAL REPORT

SUMMARY

This report compares the simulation results of a real time control algorithm for onboard computation of time-optimal intercept trajectories for the F-8 and F-15 aircraft. Due to the inherent aerodynamic and propulsion differences in the aircraft, there are major differences in their optimal trajectories. The significant difference between the two aircraft are their flight envelopes. The F-8's optimal cruise velocity is thrust limited, while the F-15's optimal cruise velocity is at the intersection of the Mach and dynamic pressure constraint boundaries. This inherent difference necessitated the development of a proportional thrust controller for use as the F-15 approaches it's optimal cruise energy. Another interesting phenomena is that the optimal climb trajectory for the F-15 is along its dynamic pressure boundary. This necessitated the use of a sub-optimal proportional vertical lift controller to track the constraint boundary.

This report documents the application of singular perturbation theory to the trajectory optimization problem, along with a summary of the control algorithms. Numerical results for the two aircraft are compared to illustrate the performance of the minimum time algorithm, and to compute the resulting flight paths. A major recommendation is that future research be directed at the application of singular perturbation methods to problems in flight mechanics where state constraints, such as a maximum dynamic pressure limit, play an important role in the analysis.

This report documents a portion of the total research effort supported under this grant. The research related to time optimal aircraft pursuit evasion can be found in [4].

TABLE OF CONTENTS

LIST OF FIGURES

SECTION 1
INTRODUCTION

There has been active research into optimizing flight path trajectories using multiple time scale separation techniques. In [1] Calise and Meorder showed that by using singular perturbation theory to separate the dynamics into fast and slow modes and then applying the optimality conditions from calculus of variations, one could obtain a closed form solution to the min-time intercept problem. What soon followed was a 3-D real-time piloted simulation and which used aerodynamic and propulsion data from the F-8 [2]. The algorithm was eventually flight tested on the NASA F-8 test aircraft at NASA Ames/Dryden Flight Research Facility [3]. The objective of this research was to modify the existing algorithm for use on an F-15 aircraft.

This report documents the results of modifying the min-time intercept algorithm from the F-8 to F-15, which represents a portion of the activity supported under this research grant. A portion of this work was conducted at NASA Ames/Dryden Flight Research Facility during the summer 1989. This report will contain four sections. The problem formulation is given in Section 2. A summary of the control algorithm is given in Section 3, which highlights the application of singular perturbation theory along with the optimality conditions derived from calculus of variations. This development could have been explained in full detail, however, in the interest of brevity only the first two boundary layer approximations will be discussed. This also coincides with the fact that a sub-optimal proportion lift controller was used on the F-15 due to the fact that the optimal trajectory rides the dynamic pressure constraint. Section 4 presents numerical results comparing the F-8 and F-15. Section 5 gives the conclusions for this work and identifies future work which needs to be accomplished prior to a flight test.

SECTION 2
PROBLEM FORMULATION

The point mass equations of motion are referenced to a horizontal, target centered, inertial coordinate frame illustrated in Fig. 1

$$\dot{x} = V\cos\gamma\cos\beta \tag{1}$$
$$\dot{y} = V\cos\gamma\sin\beta - V_T\cos\gamma_T \tag{2}$$
$$\varepsilon\dot{E} = (T-D)V / W \tag{3}$$
$$\varepsilon^2\dot{\beta} = L\sin\mu / mV\cos\gamma \tag{4}$$
$$\varepsilon^3\dot{h} = V\sin\gamma \tag{5}$$
$$\varepsilon^4\dot{\gamma} = (L\cos\mu - W\cos\gamma) / mV \tag{6}$$

These equations are valid for constant weight, thrust aligned with the flight path, and flat earth approximations. $E \equiv h + V^2 / 2g$ is the total aircraft energy per unit weight, β is the heading angle, h the altitude, γ the flight path angle, and μ the bank angle. Drag is assumed to have conventional parabolic form

$$D = qSCD_0 + KL^2 / qS, \qquad q = \rho V^2 / 2 \tag{7}$$

where q is the dynamic pressure, ρ the air density and

$$K = \eta / CL_\alpha \tag{8}$$

Lift is defined by

$$L = qSCL_\alpha\alpha \tag{9}$$

where α is the angle of attack. The control variables are L, μ, and thrust T. The objective is to find the controls L, μ, T that minimize the time to intercept a constant velocity target

$$J = \int_0^{t_f} dt \tag{10}$$

The minimization is subject to the following state and control variable constraints:

$$L \leq W\, G_{max} \tag{11}$$

$$L \leq qS\, CL_{\alpha}\alpha_{max} \tag{12}$$

$$T_{min}(h,V) \leq T_{max}(h,V) \tag{13}$$

$$q \leq q_{max},\ V \leq V_{max} \tag{14}$$

where G_{max} is the maximum load factor, α_{max} the maximum angle of attack, T_{min} and T_{max} the thrust level limits that are functions of aircraft altitude and velocity. The boundary conditions are such that the initial aircraft state is fully specified and require

$$x(t_f) = y(t_f) = 0,\ h(t_f) = h_T(t_f) \tag{15}$$

for intercept, where $h_T(t_f)$ is taken as the projected target motion in altitude

$$h_T(t_f) = h_T(0) + (V_T \sin\gamma_T)t_f \tag{16}$$

The parameter ε designates multiple time scaling used to order the dynamics [1]. The approach here is to find a solution for $\varepsilon = 1$ by an power series expansion around $\varepsilon = 0$. The boundary layers are separated by rescaling time as $\tau_i = t / \varepsilon^i$, $i = 1,...,4$, respectively, then setting $\varepsilon = 0$ in the resulting equations. A justification for this specific ordering of the dynamic equations is given in [1].

SECTION 3
SUMMARY OF CONTROL ALGORITHM

3.1 Outer Solution

In the outer solution, the controlled aircraft is assumed to be traveling on a fixed course at a constant speed, as can be seen by letting $\varepsilon \rightarrow 0$ in Eqs. (3-6). This addresses only the x and y dynamics, and the states β, h, and E take on the role of control like variables. In order to satisfy the intercept requirements, we have the following constraint

$$V \sin(\beta - \lambda) = V_T \cos\gamma_T \cos\lambda \tag{17}$$

This means that there is no relative motion allowed perpendicular to the horizontal line-of-sight axis. The optimal controls h_0 and E_0 are determined from minimizing the reduced Hamiltonian

$$H_0(E,h_1) = \lambda_{x0} V\cos\beta + \lambda_{y0}(V\sin\beta - V_T\cos\gamma_T) + 1 = 0 \tag{18}$$

and it is shown in [1] that this reduces to

$$h_0, E_0 = \arg\max_{h,E}(V) \tag{19}$$

where the maximization takes place subject to the constraints in Eqs. (11-14) and subject to the following conditions that result from setting $\varepsilon=0$ in (3-6)

$$T = D_0, \quad \mu_0 = 0, \quad \gamma_0 = 0, \quad L_0 = W \tag{20}$$

The term D_0 in (20) is drag for L = W

$$D_0 = q_0 S C_{D_0} + KW^2 / q_0 S \tag{21}$$

where

$$q_0 = \rho(h_0)V_0^2 / 2, \; V_0 = \sqrt{2g(E_0 - h_0)} \tag{22}$$

The subscript 0 denotes the zeroth or outer solution. The maximization in (19) is equivalent to finding the maximum velocity cruise point.

The cruise point solution from Eq. (19) for the F-8 and F-15 aircraft are displayed in Figs. 2 and 3, superimposed upon their flight envelopes. Note that since the F-8 is thrust limited, its

cruise point lies on the T_{max}=D contour. The F-15 is q and Mach limited, and its cruise point lies at the intersection of these constraint boundaries. Thus T does not equal T_{max} in the outer solution for the F-15.

The optimal cruise heading β_0 is computed using (17)

$$\beta_0 = \sin^{-1} (V_T \cos \gamma_T \cos \lambda / V_0) + \lambda \tag{23}$$

The costates λ_{x0} and λ_{y0}, associated with the horizontal position dynamics in the outer control solution are needed in subsequent boundary layer solutions. These take the form

$$\lambda_{x0} = -\cos \beta_0 / (V_0 - V_T \cos \gamma_T \cos \beta_0) \tag{24}$$

$$\lambda_{y0} = -\sin \beta_0 / (V_0 - V_T \cos \gamma_T \cos \beta_0) \tag{25}$$

These are determined from the optimality conditions $\partial H_0 / \partial \beta = 0$ and the condition $H_0 = 0$. It should be noted that the cruise solution for h_0 and E_0 is independent of target motion and intercept geometry. This allows these quantities to be calculated off line and stored. The only outer solution calculations performed on-line are Eqs. (23), (24), and (25).

3.2 First Boundary Layer Solution

The first boundary layer addresses only the energy dynamics. The constraints

$$\mu_1 = 0, \quad \gamma_1 = 0, \quad L_1 = W \tag{26}$$

arise from Eqs. (4-6) when the time transformation $\tau = t / \varepsilon$ is introduced and we let $\varepsilon \rightarrow 0$. The control like variables are T, h and β. The optimal β is the same as in the outer solution. Since T appears linearly in the Hamiltonian,

$$T_1 = T_{max} (h,V), \text{ when } \lambda E_1 < 0 \tag{27}$$

$$T_1 = T_{min} (h,V), \text{ when } \lambda E_1 > 0 \tag{28}$$

This corresponds roughly to an energy climb and energy descent, respectively. Optimization with respect to h yields for climb

$$h_1^c = \arg \max_h \left\{ \frac{(T_{max} - D_o)V}{V - V_o} \right\}_{E = E_{current}} \quad T_{max} \geq D_o \tag{29}$$

and descent

$$h_1^d = \arg \min_h \left\{ \frac{(T_{min} - D_o)V}{V - V_o} \right\}_{E = E_{current}} \quad T_{max} \leq D_o \tag{30}$$

The climb path to cruise for the F-8 and F-15 are superimposed on the aircraft flight envelopes in Figs. 2 and 3. The optimal descent path for both aircraft is along the q_{max} boundary. The expression for the first boundary layer costate is

$$\lambda_{E1} = -W H_0 (E, h_1) / V_1 (T_1 - D_0) \tag{31}$$

where H_0 is the outer solution Hamiltonian evaluated at the first boundary layer conditions. Since the solutions for h_1^c and h_1^d are independent of target motion, they can be precomputed and stored as a function of E. Only the energy costate variable in (31) is computed on-line.

3.3 Second Boundary Layer Solution

The second Boundary layer solution determines the optimal heading angle dynamics. Introducing the time stretching transformation $\tau = t / \varepsilon^2$ and letting $\varepsilon \rightarrow 0$ while holding the slow dynamics x, y and E fixed, yields the constraints

$$\gamma_2 = 0, \quad L^2 = L_{22}^2 + W^2 \tag{32}$$

where L is the total lift and $L_{22} = L \sin \mu$, the horizontal component of lift. The control variables are T, h and L_{22}. Assuming that all turning takes place near the initial time where $\lambda_{E1} < 0$, the optimal thrust is

$$T_2 = T_{max} (h_2, V_2) \tag{33}$$

where h_2 is the optimal commanded altitude determined by

$$h_2 = \arg \min_h \{-\rho / KV H_1 (E, h, \beta)\}|_{E=E_{current},\ \beta=\beta_{current}} \tag{34}$$

In Eq. (34) $H_1(E, h, \beta)$ is the Hamiltonian in the first boundary layer evaluated at the current

values of E, h and β. It is expressed as

$$H_1(E, h, \beta) = \lambda_{x0} V\cos\beta + \lambda_{y0} (V\sin\beta - V_T \cos\gamma_T) + \lambda_{E1} [(T - D_0)V / W] + 1 = 0 \qquad (35)$$

The solution for the horizontal lift component L_{22} is

$$L_{22} = \sqrt{-qSWH_1(E,H,\beta)/(VK\lambda_1^E)} * \text{sign}(\beta_o - \beta) \qquad (36)$$

3.4 Proportional Vertical Lift Control

An option was included in the algorithm for stopping the singular perturbation analysis after the second boundary layer, and employing a sub-optimal vertical lift solution. It was necessary in this study to use this option due to the fact that zero order singular perturbation analysis results in a steady state error when following ramp like altitude commands. Although this steady error is not a critical factor for the F-8 study in [1], it is essential to accurately track the altitude command for the F-15 since the optimal climb path lies essentially along the dynamic pressure constraint (Fig. 3). The derivation of the control logic proceeds as follows. From Eq. (5)

$$\dot{h} = V\sin\gamma \qquad (37)$$

We would like the altitude rate to track the altitude error according to proportional feedback control

$$\tau_h \dot{h} = h_2 - h. \qquad (38)$$

where τ_h is the time constant associated with the decay in altitude error. Since h_2 is not a constant command signal, but more like a ramp command, a term must be included to account for the steady state error that would otherwise result. The rate of change in h_2 can be estimated using

$$\dot{h}_2 \approx \dot{h}_1 = \frac{\partial h_1}{\partial E}\dot{E} = V_1 \sin\gamma_1 \qquad (39)$$

where $\partial h_1/\partial E$ is the slope associated with altitude with respect to E along the dynamic pressure boundary (Fig. 3). In (39) we have used the fact that $h_2(E) = h_1(E)$ when the heading error is near zero. The desired flight path angle γ_d is formed by summing γ from (37) and (38) with γ_1, from (39). Using small angle approximation for $\sin\gamma$ we have

$$\gamma_d = \frac{\dot{E}}{V_1}\frac{\partial h}{\partial E} + \frac{(h_2-h)}{\tau_h V} \tag{40}$$

With γ_d defined we can calculate the vertical lift component. Using Eq. (6)

$$\dot{\gamma} = (L_1 - W\cos\gamma) / mV = \tau_\gamma (\gamma_d - \gamma) \tag{41}$$

where τ_γ is the time constant associated with the decay in flight path angle error. As an alternative, τ_γ and τ_h can be related to a desired natural frequency and damping ratio [1]. Solving for L_1 yields

$$L_1 = mV\tau_\gamma (\gamma_d - \gamma) + W\cos\gamma \tag{42}$$

The relationship between the vertical and horizontal lift components along with the bank angle are given by

$$\mu = \arctan\frac{L_2}{L_1} \qquad L = \sqrt{L_1^2 + L_2^2} \tag{43}$$

where L_2 is the horizontal component of lift.

3.5 Proportional Cruise Thrust Control

Since the flight envelope for the F-8 has as its V_{max} cruise point at a T=D point the throttle setting was set at full throttle. This means that the F-8 will asymptotically reach its optimal cruise energy. In other words it never theoretically attains the desired optimal cruise energy. The F-15 flight envelope has as its V_{max} cruise point at the intersection of the q_{max} limit and M_{max} limit. With the cruise point at this location the F-15 reaches its optimal cruise energy in finite time. By virtue of its high T/W ratio the F-15 can gain energy at a much higher rate compared to that of the F-8. Therefore in the case of the F-15 it is necessary to throttle back as the cruise energy is approached. This throttling was incorporated into the algorithm by use of a proportional controller, the derivation of which is described as follows. Since it is desired that the energy rate track the error in energy, which is constant during cruise, we have from Eq. (3)

$$\dot{E} = (T-D)\, V / W = (E_c - E)/\tau_E \tag{44}$$

Solving for T gives

$$T = W (E_c - E) / \tau_E V + D \tag{45}$$

where τ_E is the controller time constant set to give the desired rate of decay in the energy error.

The procedure for throttle control during descent was the same as that used in the F-8 study described in [1]

SECTION 4
NUMERICAL RESULTS

Figures 4 and 5 show the ground tracks for Cases 1-3. Both simulations have the same initial geometry. The target flies at a constant altitude, velocity and heading but with differing downrange initial distances. These differing initial distances demonstrate the algorithms range-matching calculation of an optimal pseudo-cruise point [1]. Notice the rapid closure rate of the F-15 as compared to the F-8. Figures 6 and 7 show the altitude and optimal commanded altitude (h_2) time histories. The time constants τ_h and τ_γ were set to correspond to a damping ratio and natural frequency of 1.0 and 0.1 respectively. Case 1 is a long range intercept which is comprised of three phases; an initial climb along the optimal climb path followed by a cruise leg at the aircraft's optimal cruise energy (E*, h*), then a descent portion along the dynamic pressure boundary to intercept the target. Cases 2-3 being shorter intercepts never obtain their optimal cruise energies due to their proximity to their targets. These cases obtain pseudo-cruise energies instead [1]. In these cases the aircraft climbs to a pseudo-cruise energy and immediately initiates descent. Notice in each of the F-8 simulations the optimal commanded altitude has peaks between 150 and 175 seconds for each case. These demonstrate the characteristic dive in the transonic region. In contrast, the F-15 has enough thrust to simply ride the dynamic pressure boundary. Another interesting feature can be seen in comparing the Case 2 time histories. The F-8 never reaches its optimal cruise energy. Instead it approaches a lower pseudo-cruise energy. The F-15 has sufficient energy rate capacity to reach its optimal cruise energy at this shorter intercept range. The Case 2 optimal climb paths are compared in Figs. 8 and 9. In the F-8 simulation notice the near constant velocity energy climb followed by the characteristic transonic dive. The F-15 climb profile is along the dynamic pressure boundary. There exists a slight dynamic pressure boundary violation in the figure, however, this can be improved by tuning the gains τ_h, τ_γ and τ_E

Figure 10 is a comparison of optimizing the h and γ dynamics [1] versus using the sub-optimal proportional lift controller. Notice the underdamped response of the optimized boundary layers results in severe dynamic pressure constraint boundary violations. This is due to separating the h and γ dynamics into separate boundary layers which has to be done in order to obtain a closed form solution. The suboptimal proportional lift controller allows the designer to pick the gains so as to avoid a q_{max} violation. Figures 11 and 12 show the flight path angle and desired flight path angle time histories. In both simulations, descent initiation is clearly evident by the sudden decrease in the desired flight path angle. Also notice that the flight path angle never exceeds 0.2 rad during climb, which validates the $\gamma = 0$ approximation in the first and second boundary layer

analysis. It can also be seen that the F-15 completes the intercept in nearly half the time it takes the F-8. The lift and bank angle profiles are shown in Figs. 13 and 14. Note that both aircraft bank 180 degrees in order to initiate descent. In the F-15 simulation, the sudden decrease in lift at 115 seconds is due to the approaching optimal cruise velocity, where the throttle control in (45) is initiated. This changes the energy rate term in (40), and consequently the vertical lift calculated in (42). In Figs. 15 and 16 the thrust histories for each aircraft are given. The time constant τ_E here was set to 6 seconds. Descent initiation is evident by the sharp decrease in thrust at 150 and 350 seconds for the F-15 and F-8 respectively. In the F-15 simulation, at 115 seconds the proportional thrust controller throttles back the engines just prior to the aircraft obtaining its pseudo-cruise energy level.

The ground tracks for Case 4 are given in Figs. 17 and 18. This case is a close in intercept which has the target moving at constant altitude, velocity and heading 180 degrees in the opposite direction. This case illustrates a combined initial hard turn and climb (yo-yo maneuver) followed by a descent under near tail chase conditions. The pursuer's initial altitude is identical to that of the target and the velocity is above the corner velocity for that altitude. Note that the downrange intercept distance is considerably less for the F-15 aircraft. Figures 19 and 20 give the altitude and commanded altitude time histories. Both aircraft perform a high speed yo-yo maneuver in order to trade speed for increased turning performance. It is interesting to note that the time to complete the hard turn is nearly identical for both aircraft, 10 seconds. The reason for the large altitude command is due to the large initial heading errors. The jump in commanded altitude is at the completion of the hard turn so as to get on the optimal climb path. Between 10 and 20 seconds the F-8 dives to trade potential energy for kinetic energy, while the F-15 just accelerates to intercept. Figures 21 and 22 show altitude versus velocity plots for Case 4 where the high speed yo-yo maneuvers are more evident. Both simulations show the aircraft moving initially toward the corner velocity to trade speed for increased turning performance. Once the turn is completed both aircraft move to get on the optimal climb path which is followed by a descent along the dynamic pressure boundary. Figures 23 and 24 show the lift and bank angle profiles. Both aircraft initiate maximum G turns at 0-10 seconds to reduce the heading error. This is followed by a climb phase followed by cruise then descent at 40 and 90 seconds for the F-15 and F-8 respectively. In the F-15 simulation it is evident that throttling is taking place at 28 seconds due to the decrease in lift. Also note the large lift at interception, this indicates that the F-15 is tending to miss the target. This is due to the higher degree of coupling in the dynamics for the F-15, which requires further investigation.

SECTION 5
CONCLUSIONS AND FUTURE RESEARCH

The differences in the numerical results between the F-8 and F-15 trajectories lie mainly in each aircraft's ability to gain energy. The F-8 is an aircraft which never encounters any state constraint boundaries during its climb phase. The F-15's higher thrust to weight ratio allows the aircraft to gain energy at a much higher rate. Since the F-15's flight trajectory lies on the dynamic pressure boundary, the methodology for optimizing the altitude and flight path angle dynamics in [1] does not apply. This was circumvented by the application of the sub-optimal proportional lift and thrust controllers which provided an adequate sub-optimal solution. It was noticed that setting the time constants τ_h, τ_γ and τ_E to achieve the best performance for long range intercepts gave poor close-in intercept performance. This problem would imply that these gains are maneuver dependent, which it not satisfactory for real time implementation. A solution to this problem is to attempt to optimize the altitude and flight path angle dynamics, subject to the dynamic pressure constraint.

The major recommendation for future research is that the singular perturbation methodology in [1] be extended to address the issue of state constrained optimization problems. This would avoid the gain scheduling issue described above. Another interesting point worth investigating is the assumption of thrust aligned along the velocity vector. Thrust is actually aligned with the body axis. This reduces the thrust component due to the angle of attack dependence that would appear in the energy rate equation.

REFERENCES

1. Calise, A. J., and Moerder, DD. D., " Singular Perturbation Techniques for Real-Time Aircraft Trajectory Optimization and Control," NASA CR-3597, August 1982.

2. Calise, A. J., Moerder, DD. D., and Price, D. B., " Piloted Simulation of an Onboard Trajectory Optimization Algorithm," *Journal of Guidance and Control*, Vol. 7, No. 3, May-June 1984, pp. 355-360.

3. Jones, F. P., Duke, E. L., and Calise, A. J., "Flight Test Experience from a Three-Dimensional Optimal Intercept of a Maneuvering Target," 2nd International Symposium on Differential Games, Williamsburg, VA, August 1986.

4. Menon, P. K., and Duke, E. L., " Time Optimal Aircraft Pursuit-Evasion with a Weapon Envelope Constraint-Final Report," Georgia Institute of Technology, January 1990.

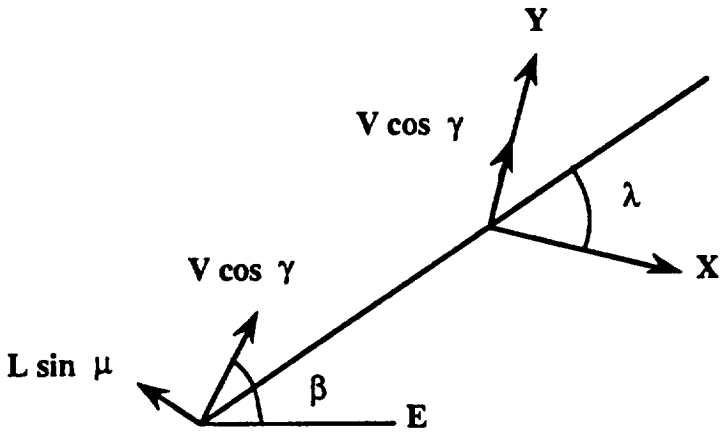

Figure 1. Horizontal plane intercept geometry

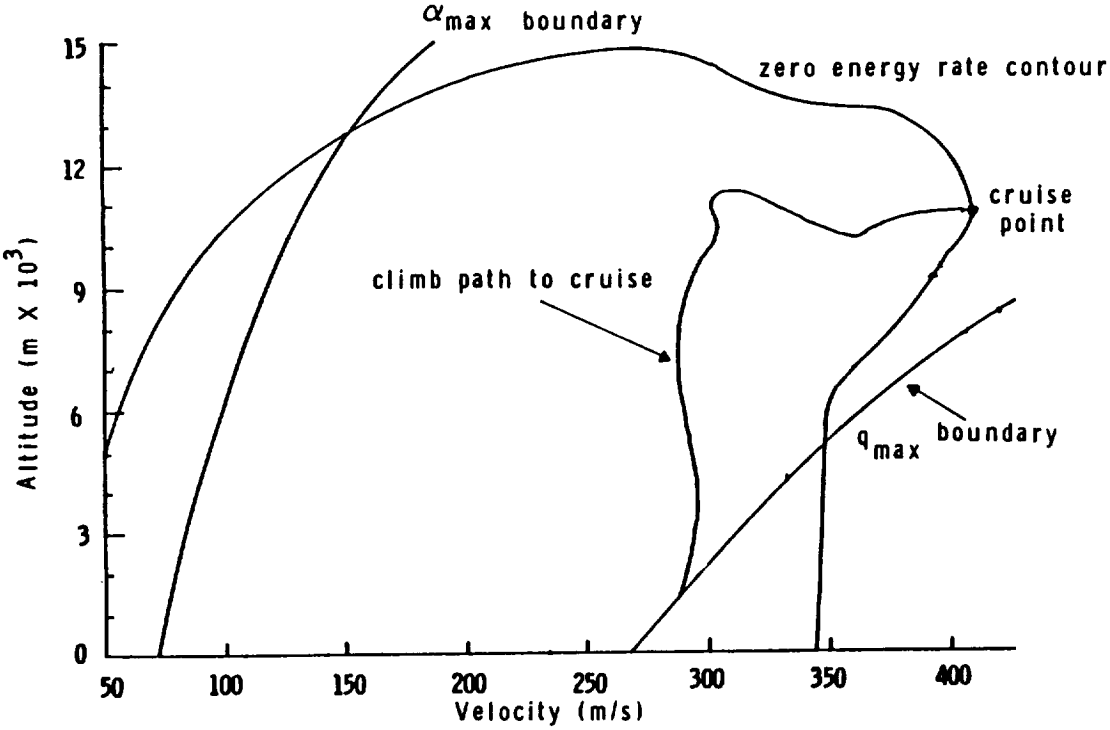

Figure 2. Flight envelope for the F-8 aircraft

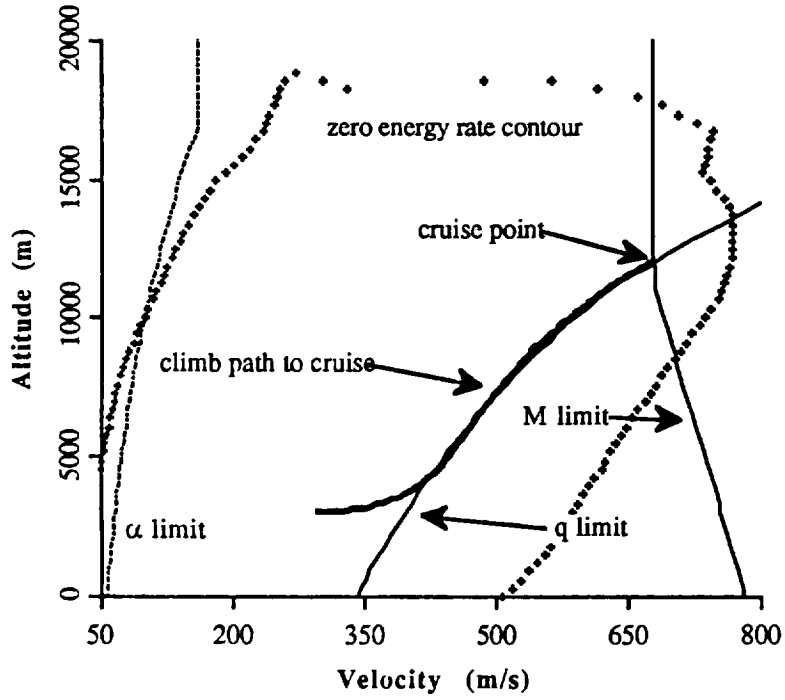

Figure 3. Flight envelope for the F-15 aircraft

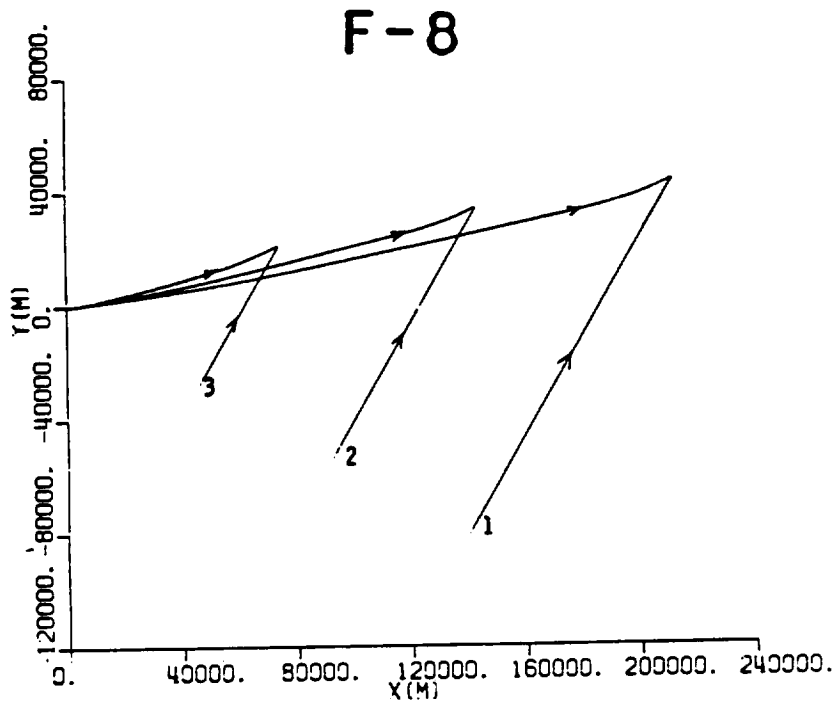

Figure 4. Ground tracks for cases 1-3

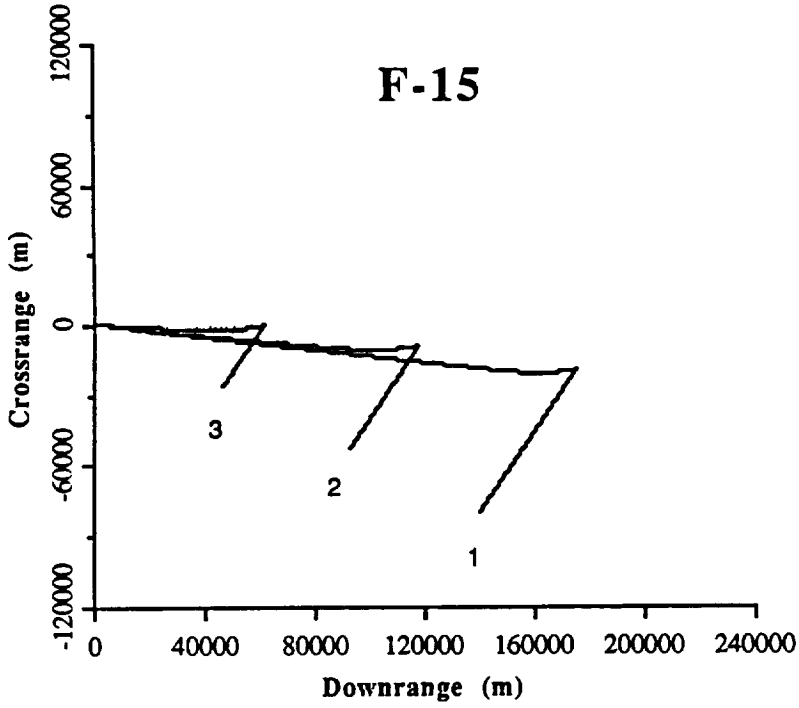

Figure 5. Ground tracks for cases 1-3

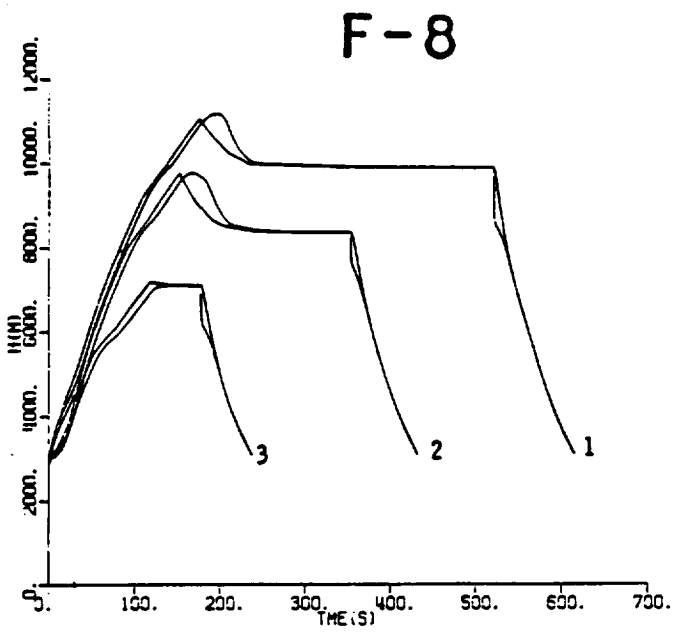

Figure 6. Commanded and actual altitude profiles for cases 1-3

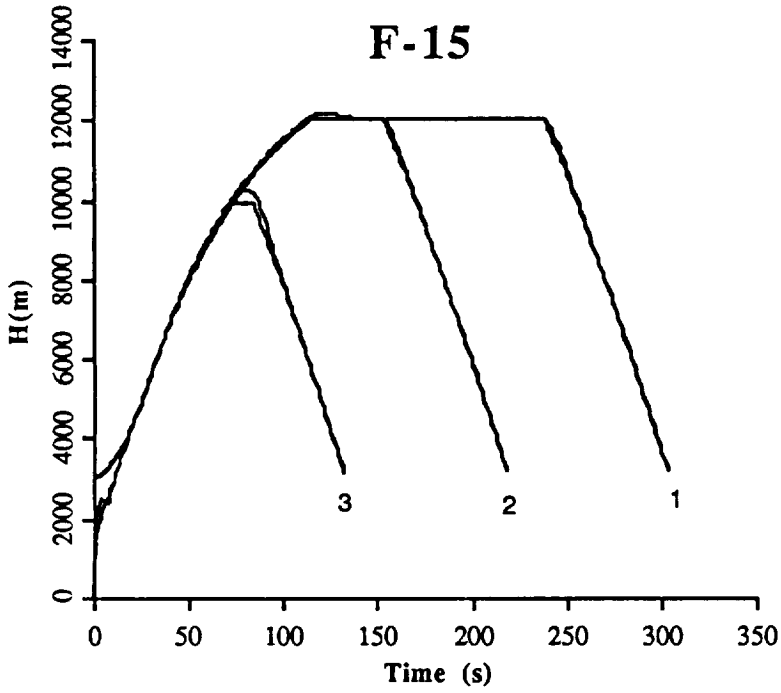

Figure 7. Commanded and actual altitude profiles for cases 1-3

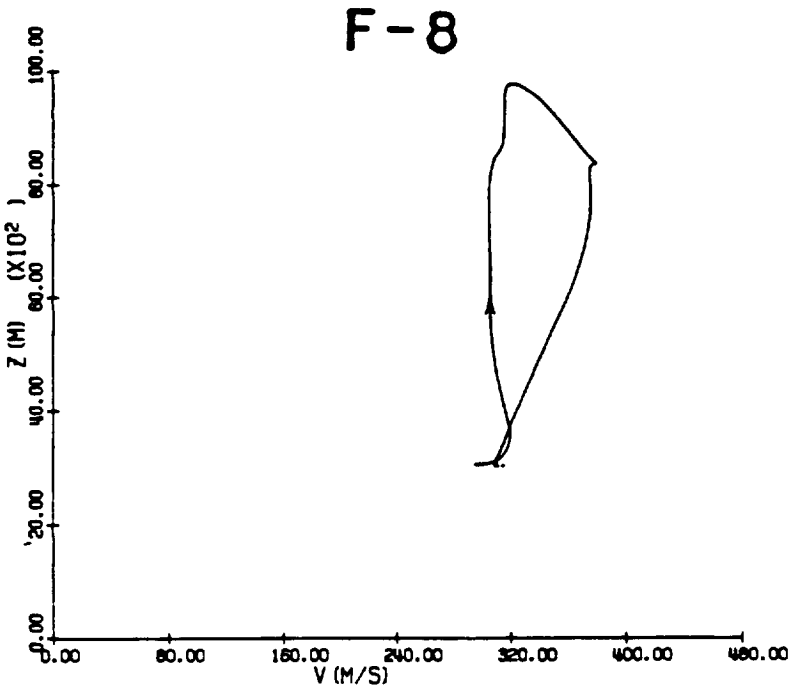

Figure 8. Altitude versus velocity for case 2

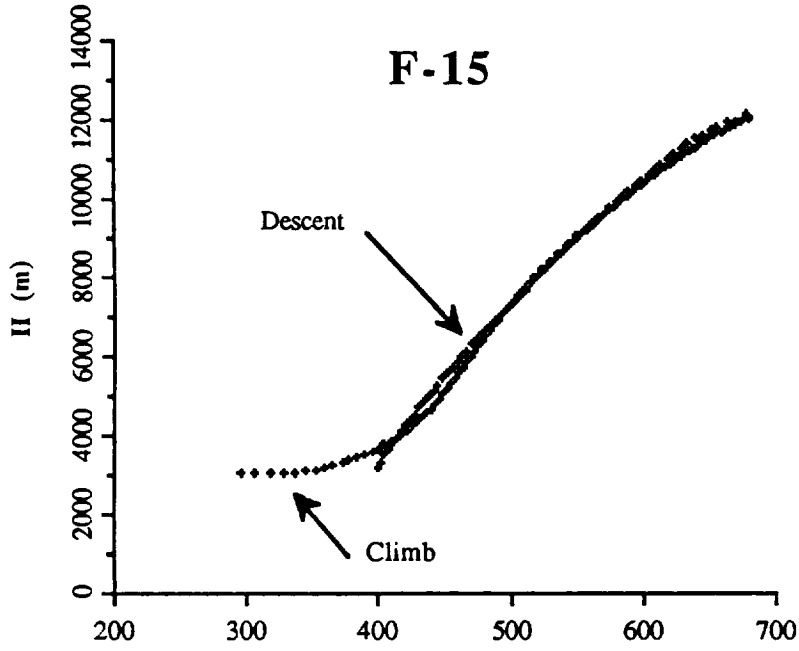

Figure 9. Altitude versus velocity for case 2

Comparison of Numerical Results:

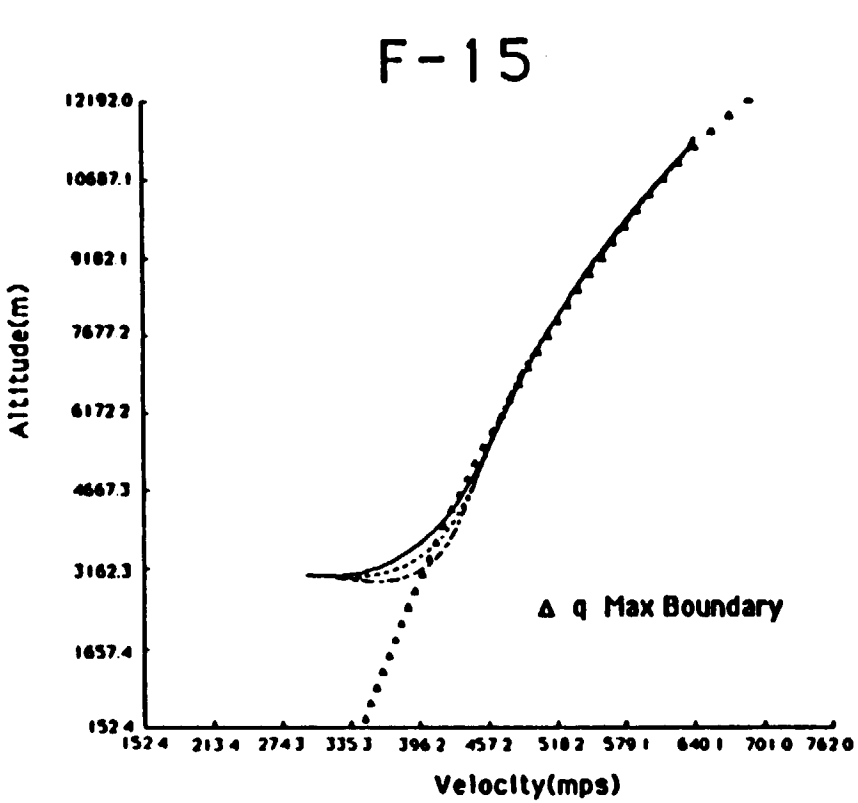

Altitude vs Velocity for 3 values of Ωn and ζ

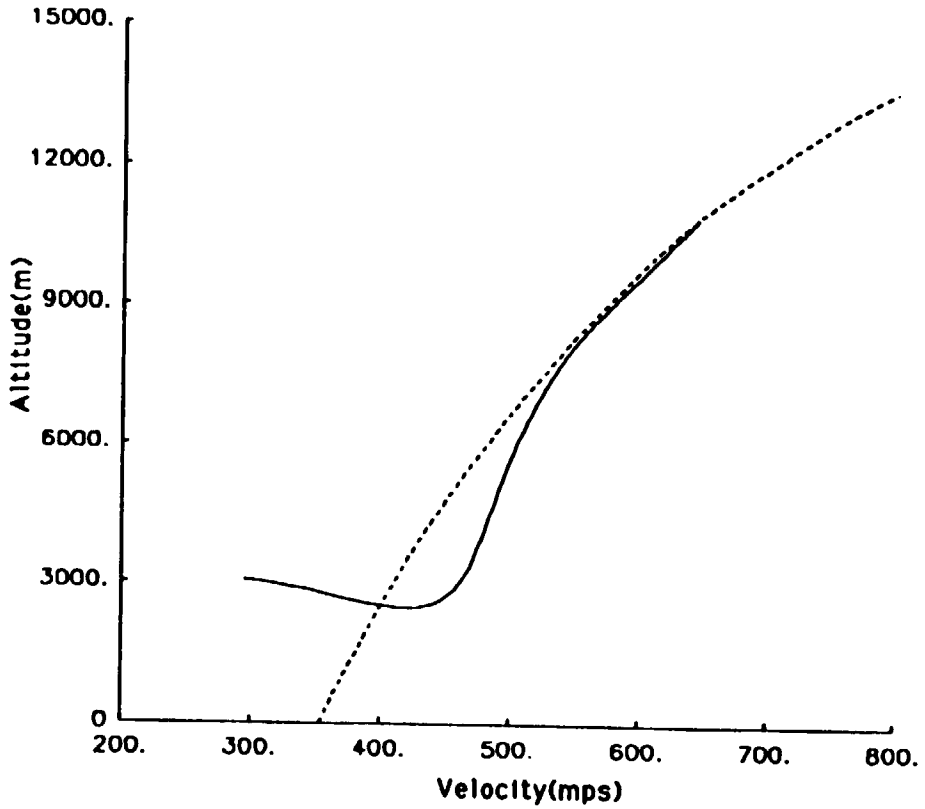

Altitude vs Velocity for 3rd and 4th Boundary Layer Optimization

——— $\zeta = 1.00$ $t_s = 22.5$ sec
- - - - - - - $\zeta = 0.85$ $t_s = 22.5$ sec
—·— $\zeta = 0.70$ $t_s = 22.5$ sec

Figure 10. Comparison of full boundary layer optimization with sub-optimal proportional lift controller

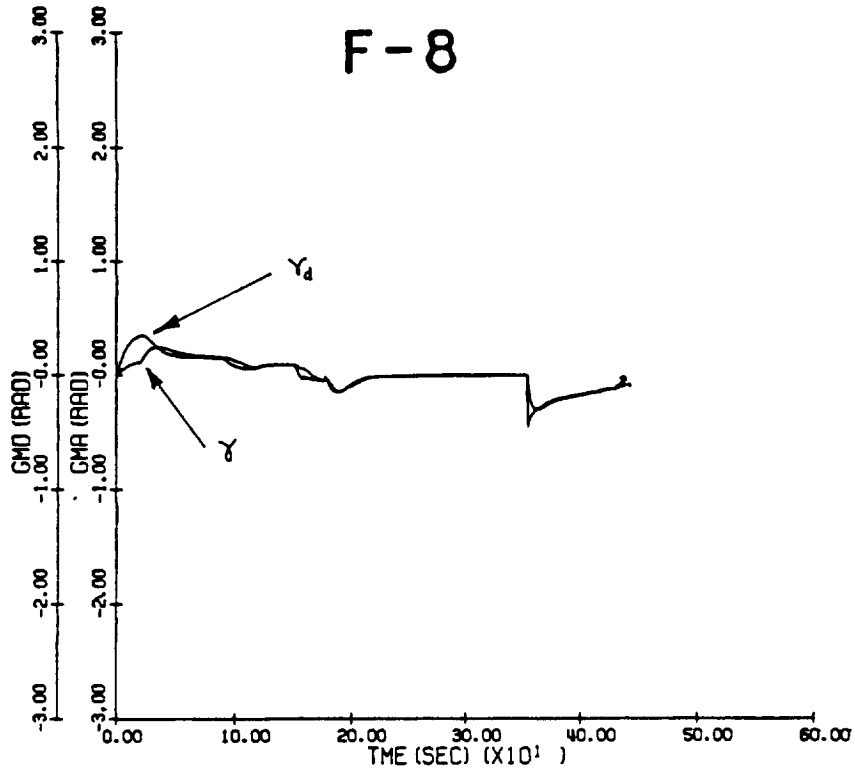

Figure 11. Desired and actual flight path angle profile for case 2

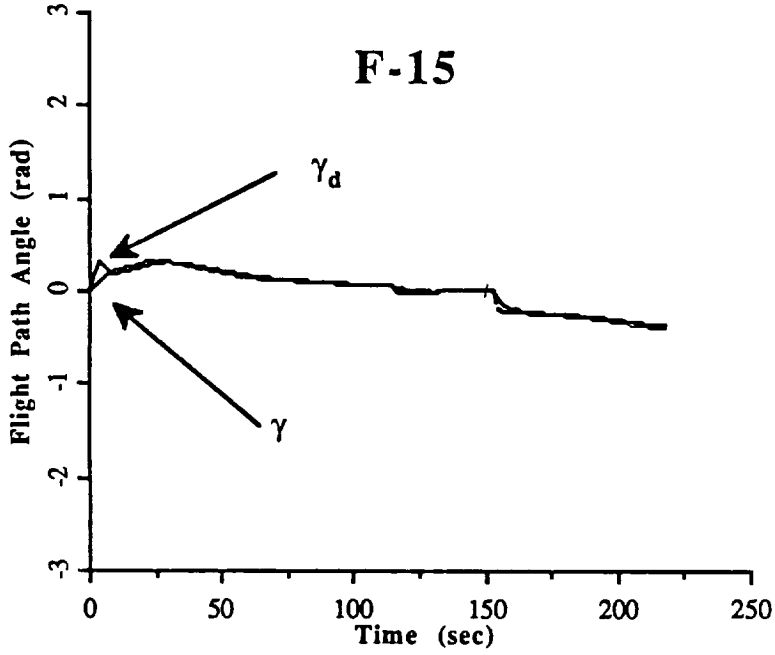

Figure 12. Desired and actual flight path angle profile for case 2

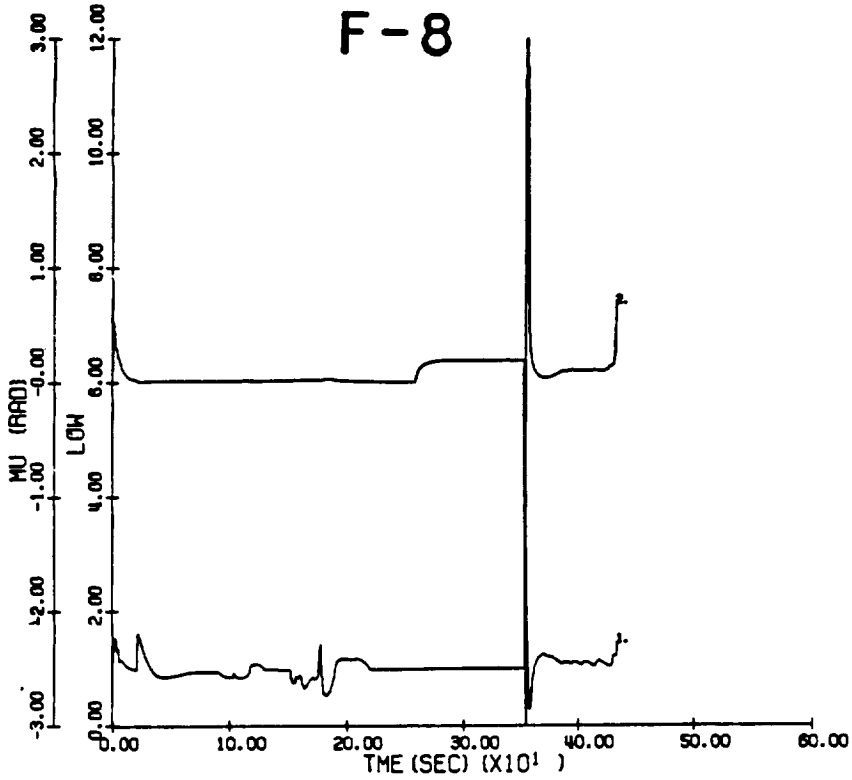

Figure 13. Lift and bank angle profile for case2

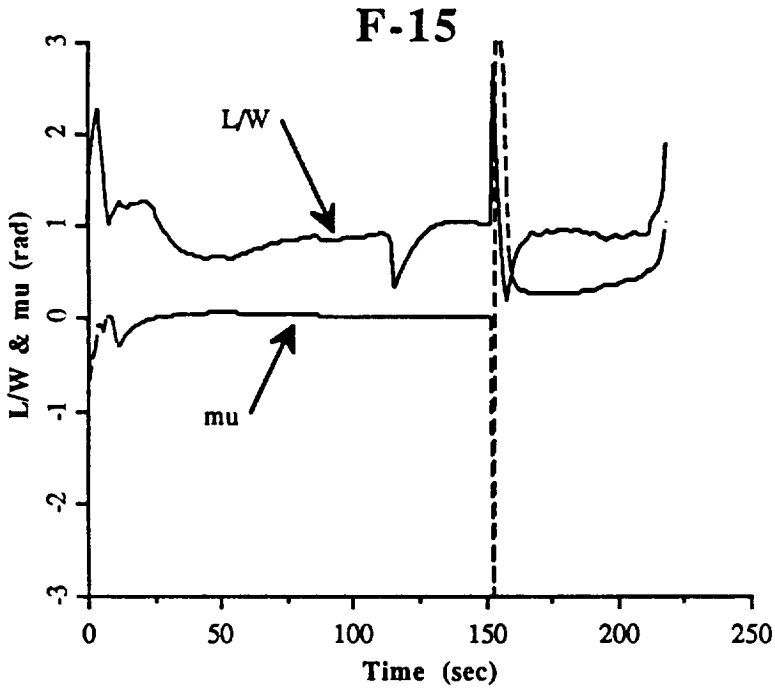

Figure 14. Lift and bank angle profile for case 2

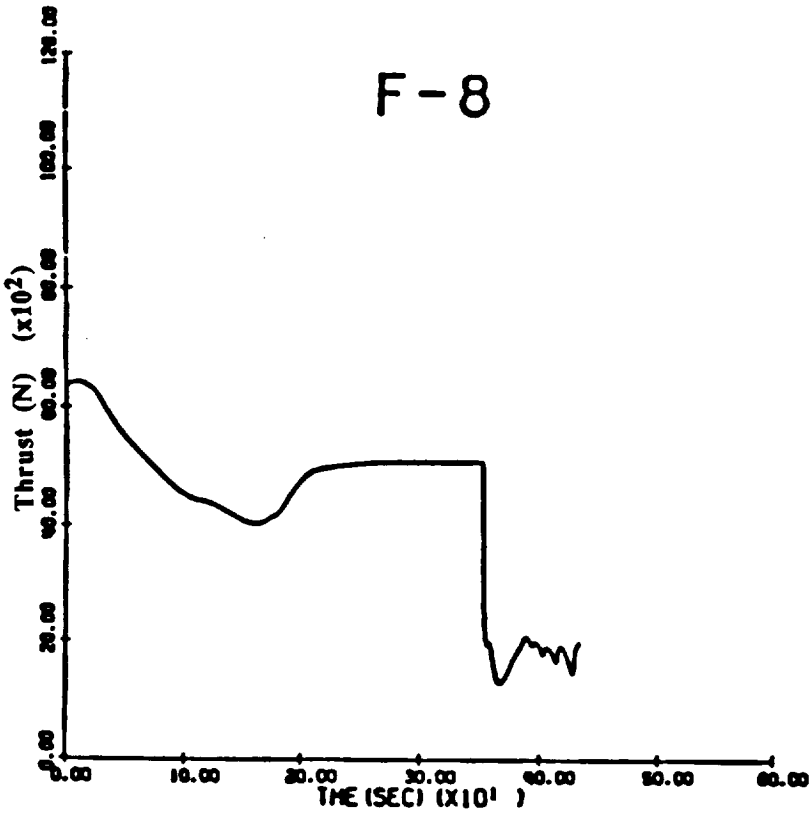

Figure 15. Thrust profile for case 2

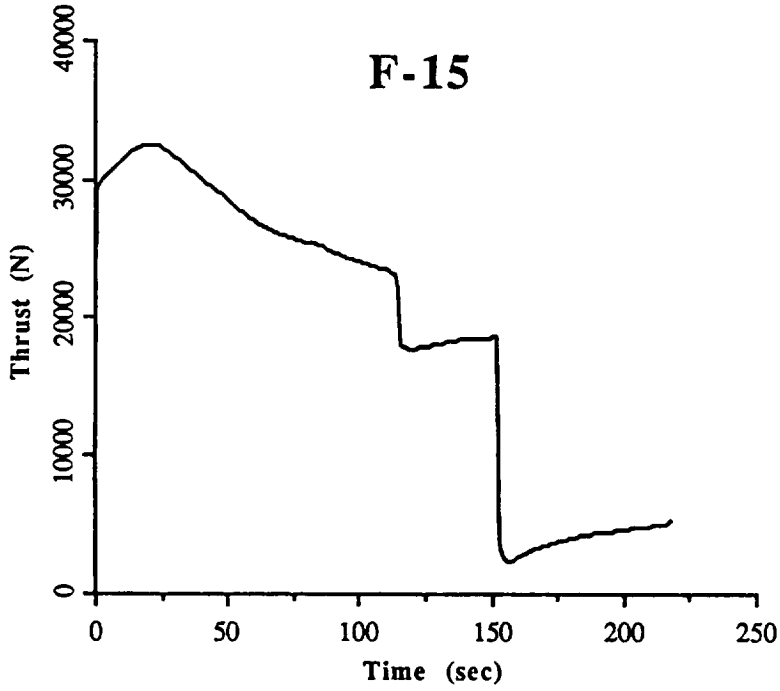

Figure 16. Thrust profile for case 2

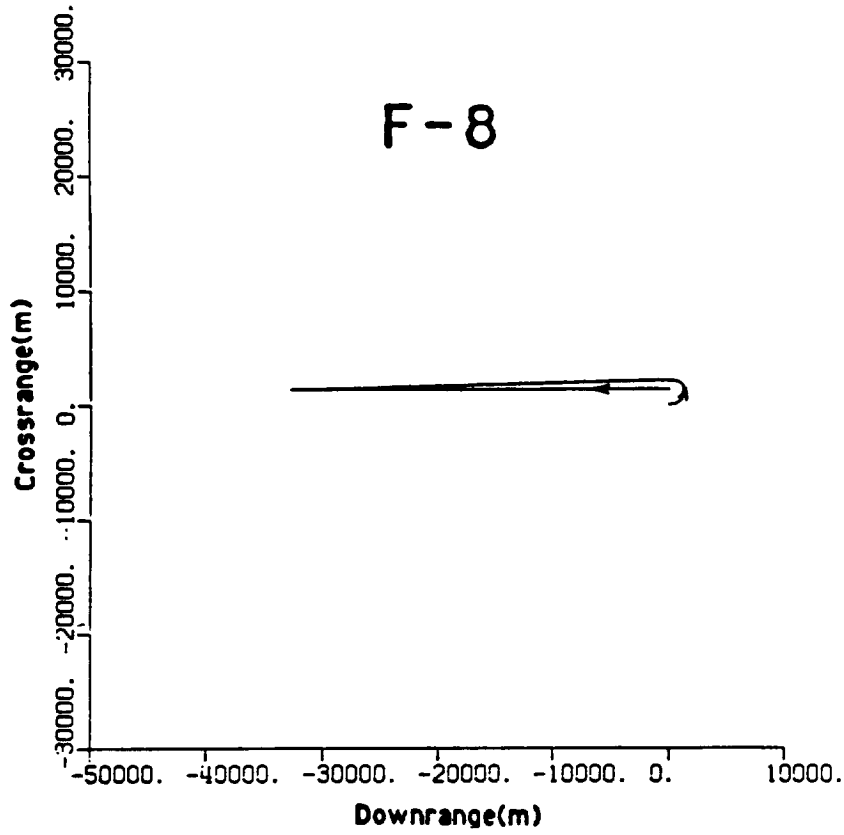

Figure 17. Ground track for case 4

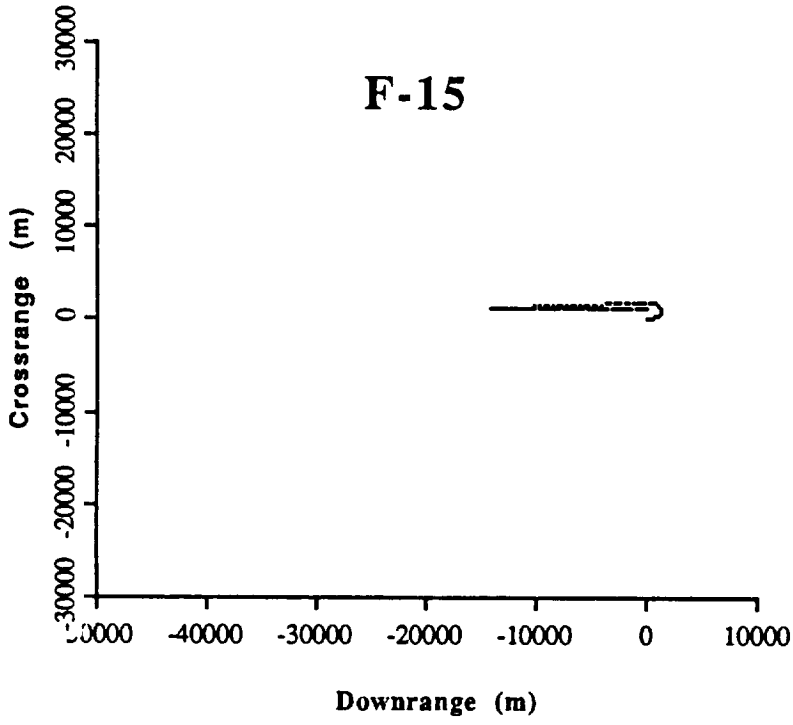

Figure 18. Ground track for case 4

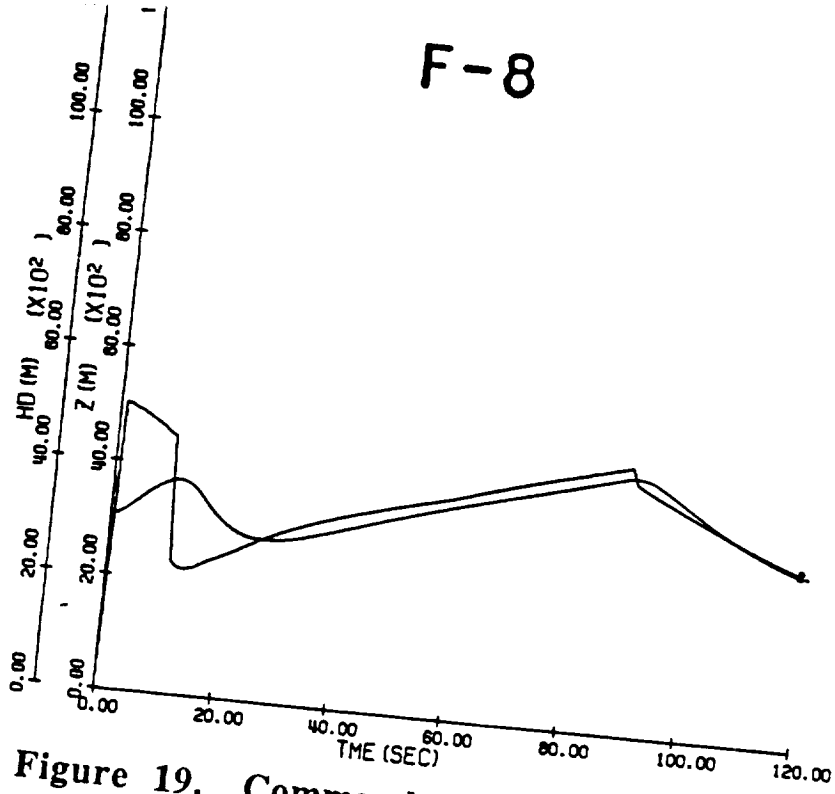

Figure 19. Commanded and actual altitude profiles for case 4

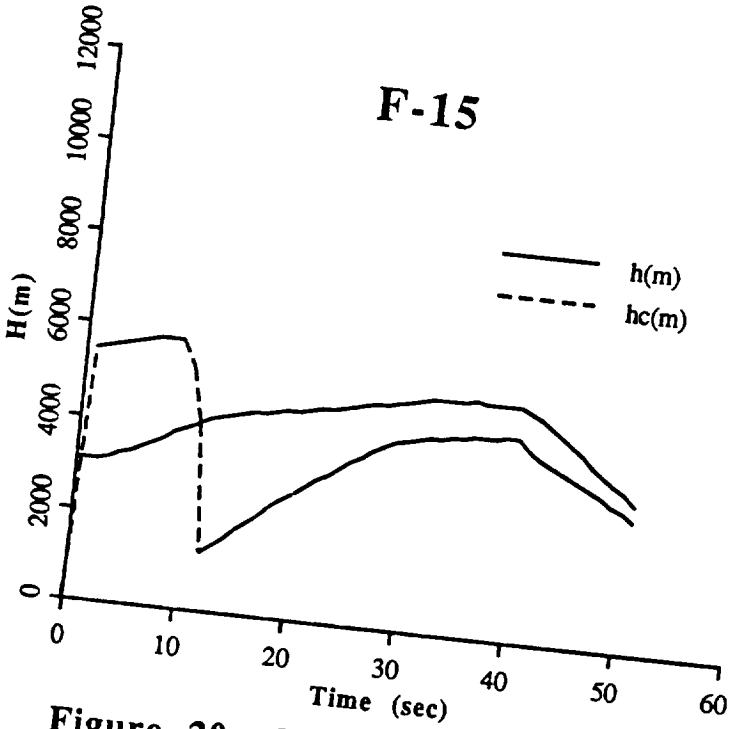

Figure 20. Commanded and actual altitude profiles for case 4

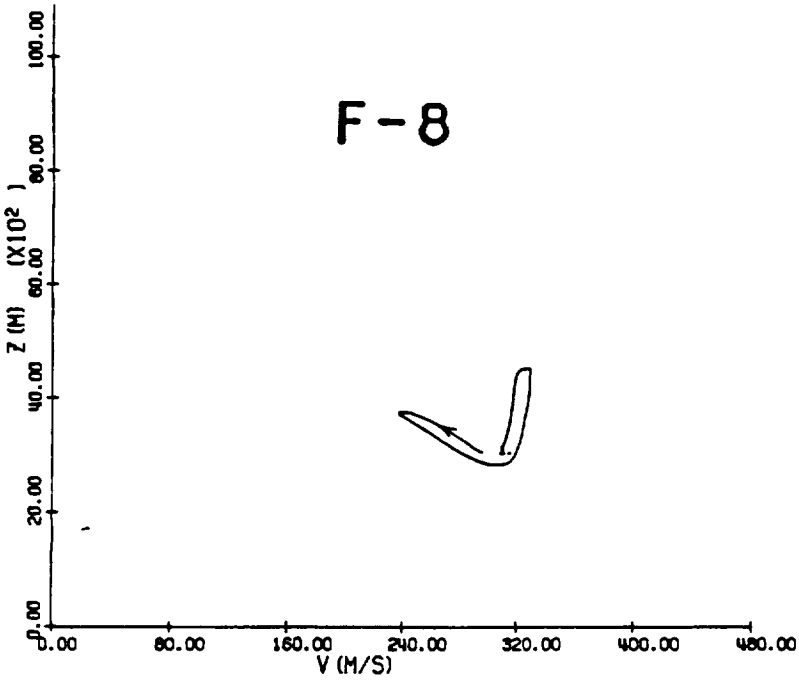

Figure 21. Altitude versus velocity for case 4

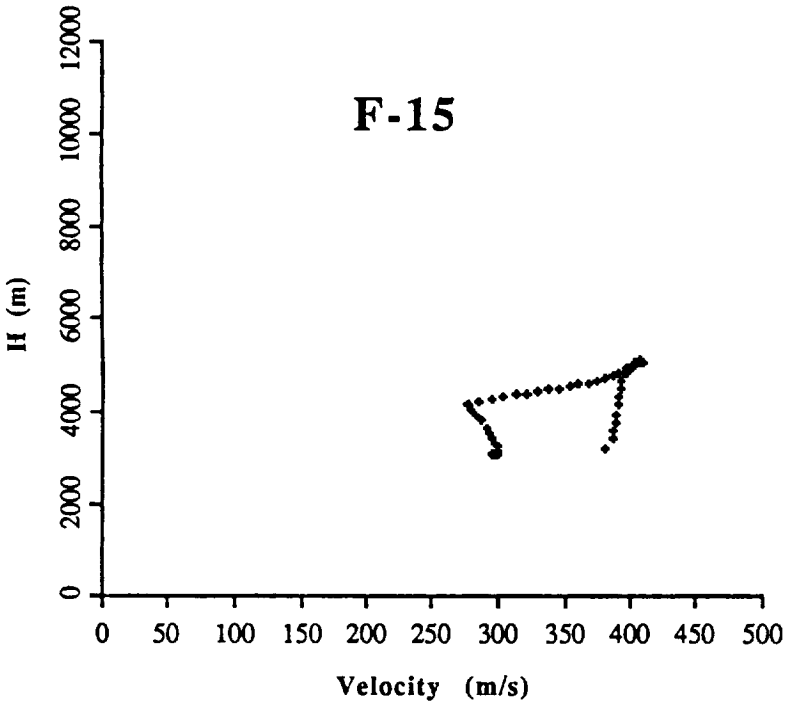

Figure 22 Altitude versus velocity for case 4

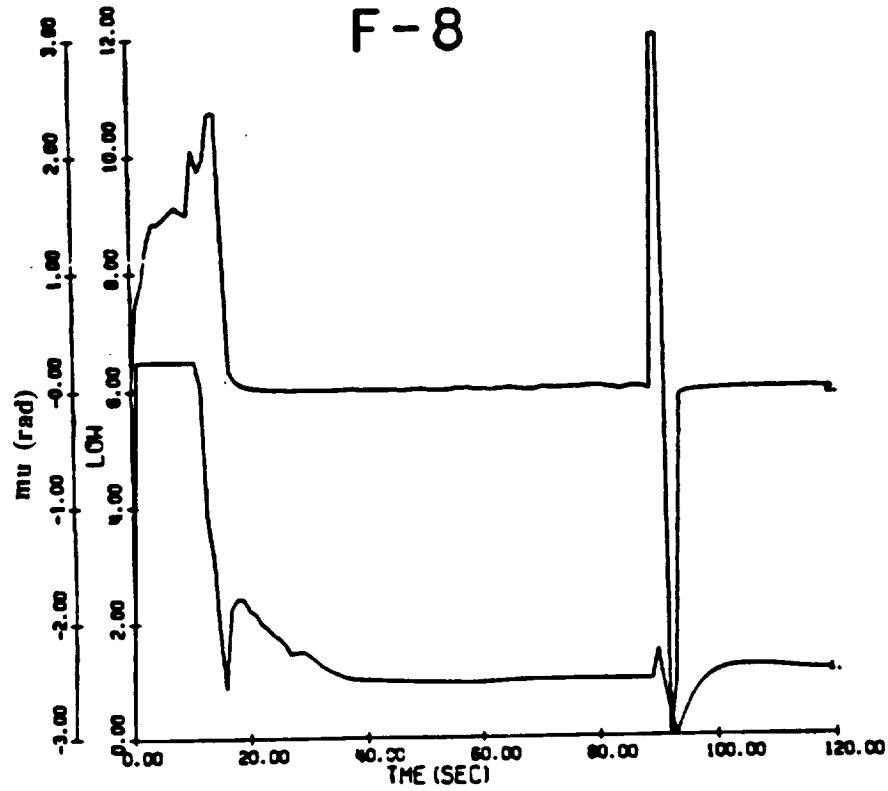

Figure 23. Lift and bank angle profile for case 4

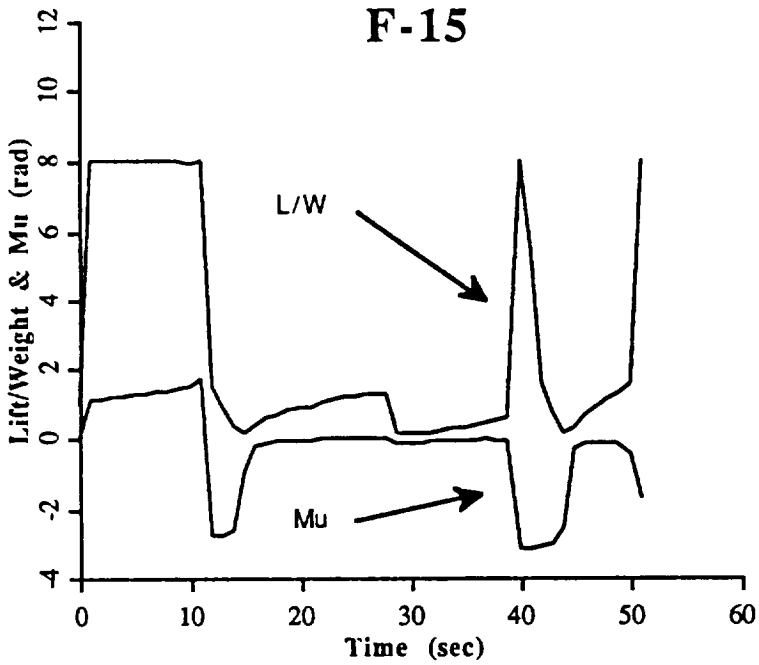

Figure 24. Lift and bank angle profile for case 4